Probing Superatomic Orbitals of Sc-Doped and Undoped Silver Cluster Anions via Photoelectron Angular Anisotropy

Minamikawa, K.
Department of Chemistry, Faculty of Science, Kyushu University

Nishizato, T.
Department of Chemistry, Faculty of Science, Kyushu University

Hashimoto, H.
Department of Chemistry, Faculty of Science, Kyushu University

Matsumoto, K.
Department of Chemistry, Faculty of Science, Kyushu University

他

出版情報：The Journal of Physical Chemistry Letters. 14 (17), pp.4011-4018, 2023-04-21. American Chemical Society
バージョン：

Probing Superatomic Orbitals of Sc-doped and Undoped Silver Cluster Anions via Photoelectron Angular Anisotropy

K. Minamikawa,[†] T. Nishizato, [†] H. Hashimoto, K. Matsumoto, M. Arakawa, T. Horio, and A. Terasaki**

Department of Chemistry, Faculty of Science, Kyushu University, 744 Motooka, Nishi-ku, Fukuoka 819-0395, Japan

Corresponding Authors

*horio@chem.kyushu-univ.jp, *terasaki@chem.kyushu-univ.jp

[†]These authors contributed equally.

Abstract

Valence s electrons in alkali- or coinage-metal clusters are conceived to delocalize over the metal frameworks. The electrons occupy so-called superatomic orbitals (SAOs, i.e. 1S, 1P, 1D, 2S, 1F, …), which provide an essential picture for understanding the size-dependent, unique properties of these metal clusters. While such electronic shells are unambiguously identified in their photoelectron spectra and supported by electronic structure calculations, characterization of SAOs in heteroatom-doped metal clusters has remained elusive as the doping significantly affects its energy levels and even alters the ordering of SAOs. Here, we present a photoelectron imaging study to explore SAOs formed in Sc-doped and undoped silver cluster anions, Ag_NSc^- (N = 15, 16) and Ag_N^- (N = 18, 19). Photoelectron angular distributions from their outermost SAOs are clearly visualized, whose characters are analyzed with the aid of density functional theory calculations. The present methodology enables us to explore not only the quantized energy levels but also the spatial distributions of SAOs formed in various metal cluster anions.

TOC GRAPHICS

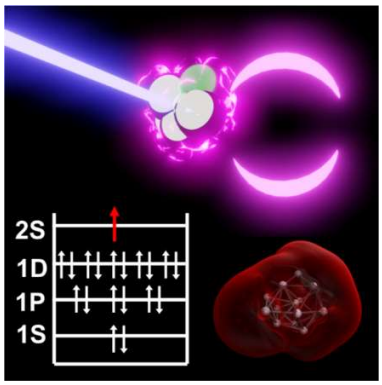

KEYWORDS

Metal clusters, Superatomic orbitals, Jellium model, Photoelectron imaging, Photoelectron angular anisotropy

Since the work by Knight et al., [1] valence s electrons in alkali- and coinage-metal clusters have been conceived to move freely over the metal frameworks. The jellium model successfully explains this picture,[2] where these metal clusters are expected to have atomic-like electronic shells of 1S, 1P, 1D, 2S, 1F, …. The discrete energy levels are often termed as superatomic orbitals (SAOs), which have indeed been identified in their photoelectron spectra.[3–8] Note that the difference between SAOs and ordinary atomic orbitals (1s, 2s, 2p, 3s, 3p, 3d, …) in principal and angular momentum quantum numbers is due to their different potential fields: quantum well and Coulomb potentials. The concept of SAOs is now essential for understanding their size-dependent properties, discovering unique metal clusters called "superatoms",[9] and rationally designing functional materials based on superatoms in solutions.[10]

The success of the jellium model raised a fundamental issue of its applicability to bimetallic clusters. Kappes et al.[11] addressed this issue by measuring photoionization mass spectra of K_xLi, K_xMg, and K_xZn, where the authors found large relative abundances of K_7Li^+, K_8Mg^+, and K_8Zn^+. While the result for K_7Li^+ suggests that K_7Li has an electronic shell closing with $1S^21P^6$, the authors have proposed for K_8Mg and K_8Zn that the energy levels of 1D and 2S are reversed upon the foreign-atom doping, so that they are electronically stable with 10 valence electrons: $1S^21P^62S^2$. Nakajima et al.[12] explored ionization energies (IEs) of Al_nNa_m and found large IEs for $Al_{13}Na$ and $Al_{23}Na$ compared to those for the neighboring sizes containing a single sodium atom, although Na works as a dopant in these systems. The results suggest that the doped clusters have a closed electronic shell, where 3s and 3p electrons of Al also contribute to electron counting in the formation of SAOs: $Al_{13}Na$ (40 valence electrons) and $Al_{23}Na$ (70 valence electrons) have 2P and 3S electronic shell closings, respectively. These pioneering studies have stimulated a continuous effort to characterize valence electronic structures of bimetallic clusters.

As for doped coinage-metal clusters, density functional theory (DFT) calculations by Pyykkö and Runeberg proposed an icosahedral gold cage encapsulating tungsten, $Au_{12}W$,[13] where the authors predicted that a closed electronic shell, $1S^21P^61D^{10}$, is formed with 18 valence electrons of Au and W (Au $6s^1 \times 12$ + W $5d^46s^2$), indicating that the cluster is electronically stable as well. Anion photoelectron spectroscopy (PES) for $Au_{12}W^-$ by Li et al.[14] identified a significantly sharp peak at the vertical electron detachment energy (VDE) of 2.08 eV, suggesting that the excess electron is weakly bound to a stable core of $Au_{12}W$. Relative stabilities of doped coinage-metal clusters have also been explored by Lievens and co-workers,[15,16] who presented systematic investigations into mass spectral patterns of Au_NX^+ and Ag_NX^+ (X = 3d transition metal, Sc–Ni) after ultraviolet (UV) photofragmentation. From their relative abundances, the authors proposed that $Au_{16}Sc^+$, $Au_{15}Ti^+$, $Ag_{16}Sc^+$, $Ag_{15}Ti^+$, $Ag_{14}V^+$, $Ag_{11}Fe^+$, $Ag_{10}Co^+$, and Ag_9Ni^+ should have a closed electronic shell of $1S^21P^61D^{10}$ with all valence electrons of the 3d transition metals hybridized with the valence s electrons of Au or Ag. Our chemical reactivity measurements of the doped silver cluster cations toward molecular oxygen supported this scenario,[17] extending to exploration of chemical reactivities between negative species, Ag_NX^-, and O_2,[18] where $Ag_{14}Sc^-$, $Ag_{13}Ti^-$, and $Ag_{12}V^-$ exhibited exceptionally high stabilities against O_2. This suggests that the anions should also comply with the 18-electron rule.

In the present study, we focus on Sc-doped and undoped silver cluster anions. As is often pointed out,[6] silver clusters are distinct from the other coinage-metal clusters in electronic structure since Ag 5s electrons are considered as nearly-free electrons due to the large 5s–4d energy gap, whereas those of Cu 4s and Au 6s electrons are perturbated by their close-lying 3d and 5d electrons, respectively. We highlight that the one-electron orbital energies of the 4s and 3d valence electrons of Sc, proposed by Allen and co-workers,[19] are 6.60 and 7.92 eV,

respectively, which are both close to that of silver 5s electron, 7.58 eV.[19] This implies that highly hybridized SAOs are formed in Sc-doped silver cluster anions due to strong orbital interactions between their valence electrons; this is perhaps the same point as shown by Gilmour and Gaston,[20] who revealed by DFT investigations that early-transition metals tend to delocalize their valence d-electrons for contributing to formation of SAOs. The spherical jellium model therefore simply predicts that the valence electronic structures of $Ag_{15}Sc^-$ and $Ag_{16}Sc^-$ are $1S^21P^61D^{10}2S^1$ and $1S^21P^61D^{10}2S^2$, respectively. Here, we explore these Sc-doped silver clusters and their valence isoelectronic counterparts, Ag_{18}^- and Ag_{19}^-, to visualize their outermost SAOs using the novel photoelectron imaging apparatus recently developed in our group.[21] As explained below, photoelectron angular distributions (PADs) from 2S SAO are expected to show unique characteristics, which motivated us to investigate these metal cluster anions.

In single-photon photodetachment from atomic anions with linearly-polarized light, the dipole selection rule for the orbital angular momentum quantum number (l) and the magnetic quantum number (m), i.e., $\Delta l = \pm 1$ and $\Delta m = 0$, predicts that only p_z-wave ($l = 1$, $m = 0$) is allowed from s orbitals ($l = 0$, $m = 0$), giving rise to a significant anisotropy of PAD parallel to the polarization vector of the light.[22] Figures 1(a) and (b) represent a two-dimensional (2D) projection of photoelectrons detached from Ag^- with the 404-nm (3.07-eV) CW laser, which was already reported in our recent work,[21] and the 2D slice of the photoelectron distribution reconstructed from Fig. 1(a), respectively (see EXPERIMENTAL METHODS). Since only the 5s electron of Ag^- ($[Kr]4d^{10}5s^2$) can be detached upon irradiation of the UV light, the 2D slice shown in Fig. 1(b) exhibits a single, sharp ring. The observed PAD is consistent with the aforementioned prediction. The photoelectron anisotropy parameter, β, is generally defined by the well-known formula, $I(\theta) \propto 1+(\beta/2)(3\cos^2\theta-1)$, where $I(\theta)$ is the photoelectron

intensity with respect to the polar angle, θ, from the laser polarization direction. The reconstruction procedure from Fig. 1(a) to 1(b) yielded $\beta = 2.00 \pm 0.12$; the error is the standard deviation obtained by independently analyzing each quadrant image of Fig. 1(a). Our value is in good agreement with 2 ± 0.06 measured by Sobhy and Castleman.[23]

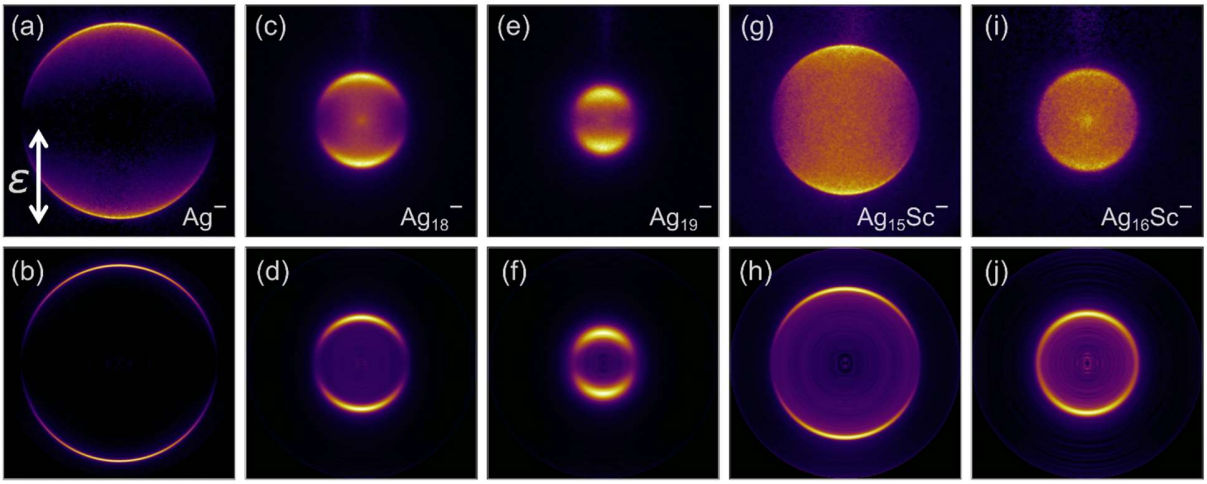

Figure 1. 2D projections (upper panels) and 2D slices (lower panels) of photoelectron distributions detached from Ag^- ((a) and (b)), Ag_{18}^- ((c) and (d)), Ag_{19}^- ((e) and (f)), $Ag_{15}Sc^-$ ((g) and (h)), and $Ag_{16}Sc^-$ ((i) and (j)). The direction of the polarization vector, ε, of the 404-nm light is indicated by a double arrow in (a).

Rigorously speaking, the above argument cannot be applied to metal cluster anions as they are not spherically symmetric in reality. Nonetheless, Bartels et al.[24] demonstrated that PAD from the 2S electrons of Na_{19}^- ($1S^2 1P^6 1D^{10} 2S^2$) in the vicinity of the photodetachment threshold exhibits significantly high positive anisotropy ($\beta = 1.3 \sim 1.6$), which is qualitatively consistent with PAD for s electrons of atomic anions. As shown in Figs. 1(c)–(f), the present study demonstrates that such anisotropic PADs also hold for photodetachment signals from 2S SAO of

Ag_{18}^- ($1S^21P^61D^{10}2S^1$) and Ag_{19}^- ($1S^21P^61D^{10}2S^2$). The β values corresponding to the VDEs (the most intense part of the sharp rings of the 2D slice images) for Ag_{18}^- (Fig. 1(d)) and Ag_{19}^- (Fig. 1(f)) are determined to be 1.52 ± 0.03 and 1.08 ± 0.06, respectively.

Here, we draw attention to the results of doped clusters, $Ag_{15}Sc^-$ and $Ag_{16}Sc^-$. It is remarkable that $Ag_{15}Sc^-$ also exhibits a highly anisotropic PAD with more electrons emitted parallel to the laser polarization vector, as shown in Figs. 1(g) and (h). The β value is as high as 1.58 ± 0.11, suggesting that the 19 valence electrons are fully delocalized in the $Ag_{15}Sc^-$ framework with $1S^21P^61D^{10}2S^1$ configuration, where the 2S electron is detached with the 404-nm light. These results for Ag_{18}^-, Ag_{19}^-, and $Ag_{15}Sc^-$ indicate that a large β value in the photodetachment threshold can be a fingerprint for the formation of 2S SAO in metal cluster anions. Note that the anisotropy of PAD for $Ag_{16}Sc^-$ diminishes with the β value of 0.62 ± 0.11; the reason for this behavior will be discussed later.

The experimental β values for all clusters investigated are summarized in Table 1 along with VDEs, which are determined from the photoelectron spectra presented in Figs. 2(a)–(d). It should be noted that our VDEs of 2.60 ± 0.02 and 2.86 ± 0.01 for Ag_{18}^- and Ag_{19}^-, respectively, are in good agreement with those measured by Handschuh et al.[6] (2.58 and 2.84 eV for Ag_{18}^- and Ag_{19}^-, respectively), where a pulsed arc discharge cluster source was employed in combination with a magnetic-bottle time-of-flight photoelectron spectrometer. VDEs evaluated by DFT calculations, which will be described below, are also presented in Table 1.

TABLE 1. Photoelectron anisotropy parameters, β, and vertical detachment energies (VDEs).

	Photoelectron anisotropy parameter, β		Vertical detachment energy (VDE) / eV	
	Expt.[a]	Calc.[b]	Expt.	Calc.
Ag_{18}^-	1.52 ± 0.03	1.95	2.60 ± 0.02	2.61
Ag_{19}^-	1.08 ± 0.06	1.77	2.86 ± 0.01	2.85
$Ag_{15}Sc^-$	1.58 ± 0.11	1.57	1.82 ± 0.02	1.97
$Ag_{16}Sc^-$	0.62 ± 0.11	1.34	2.51 ± 0.02	2.51

[a]Obtained at the VDEs. The error is the standard deviation estimated by independently analyzing each quadrant image of Figs. 1(c), (e), (g), and (i). [b]Obtained by ezDyson 5.0 (see the text).

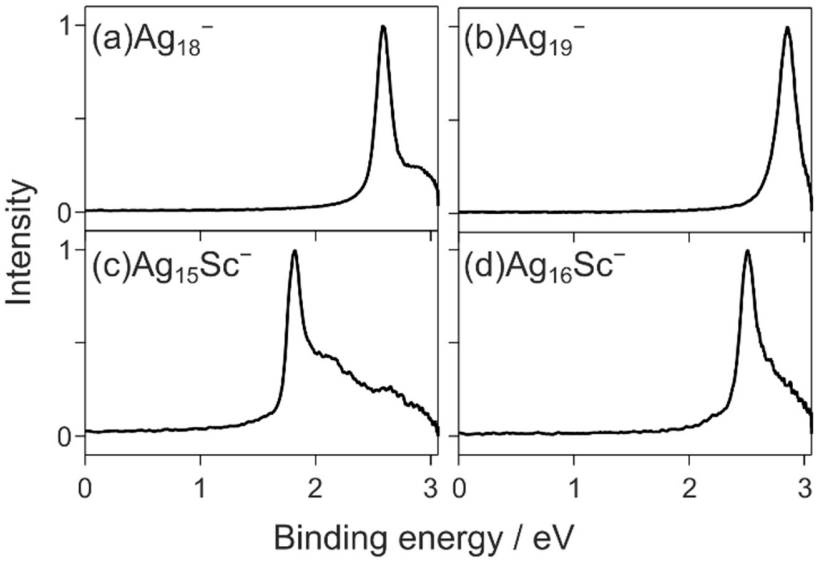

Figure 2. Photoelectron spectra of (a) Ag_{18}^-, (b) Ag_{19}^-, (c) $Ag_{15}Sc^-$, and (d) $Ag_{16}Sc^-$. The intensity is in arbitrary units.

To gain theoretical insight into the experimental β parameters, we first performed DFT calculations for exploring the most stable geometries of all the clusters. The geometry optimization was performed by the Gaussian 16 package,[25] where BP86 functional[26,27] with the basis sets of 6-311+G(d) (the Wachters-Hay all electron basis set[28,29] using the scaling factors of Raghavachari and Trucks[30]) for Sc and LanL2DZ for Ag with the corresponding effective core potential were employed.[31] As for the initial geometries of Ag_N^- (N = 18, 19), we referred to the optimized structures reported by Yin et al.[32] The optimized structures of Ag_N^- (N = 18, 19) and Ag_NSc^- (N = 15, 16) are presented in the insets of Figs. 3(a)–(d), respectively, along with the isosurface plots of Kohn-Sham orbitals and its energy levels. While the geometries of Ag_{18}^- and Ag_{19}^- are in C_{2v} and C_3 point groups, respectively, the doped clusters, $Ag_{15}Sc^-$ and $Ag_{16}Sc^-$ belong to C_s and C_1, respectively; the structures of Ag_N^- (N = 18, 19) almost reproduce those obtained by Yin et al. The calculations have revealed that the spin states of Ag_{18}^- and $Ag_{15}Sc^-$ are doublet and those of Ag_{19}^- and $Ag_{16}Sc^-$ are singlet.

After the geometrical optimization, we evaluated their VDEs, which were obtained by the total energy difference between the anions and the corresponding neutrals in their ground electronic states that have exactly the same geometries as the anions. The calculated VDEs, summarized in Table 1, well reproduce the experimental values, which rationalizes the optimized geometries for all the clusters. It should be noted in Figs. 3(a)–(d) that the orbital energies are shifted such that the shifted energies of the highest occupied molecular orbitals (HOMOs) exactly match the negative signs of the experimental VDEs; the energy shift relies on generalized Koopmans' theorem,[33] which has been employed to simulate peak energies of experimental photoelectron spectra using Kohn-Sham orbital energies.[34] Also note that the photoelectron spectra shown in Figs. 2(a)–(d) are superimposed on Figs. 3(a)–(d), respectively.

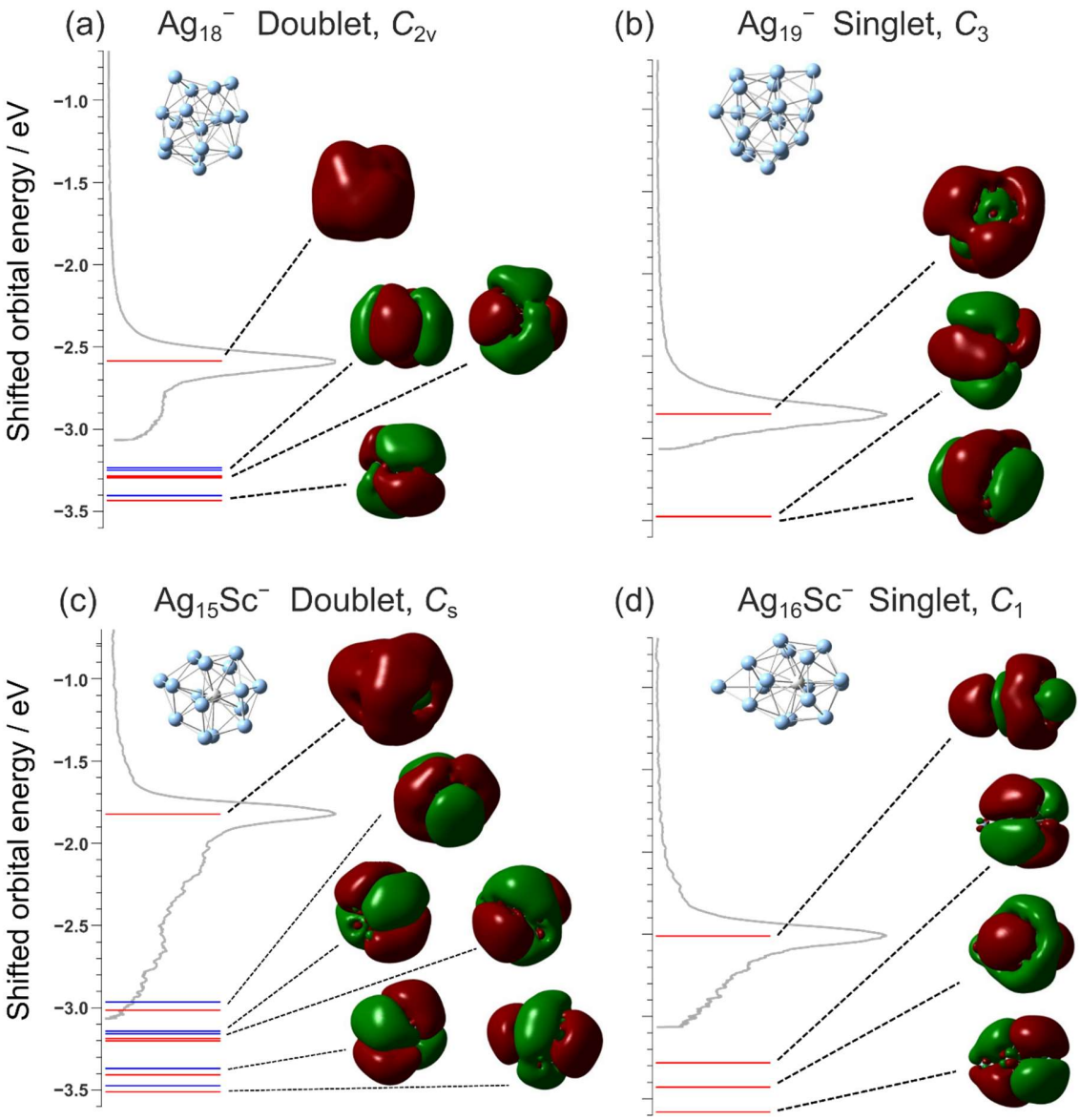

Figure 3. Optimized structures, isosurface plots of Kohn-Sham orbitals, and its energy levels of (a) Ag_{18}^-, (b) Ag_{19}^-, (c) $Ag_{15}Sc^-$, and (d) $Ag_{16}Sc^-$. The orbital energies, which are shown with red (alpha electrons) and blue (beta electrons) horizontal lines, are shifted so that the calculated orbital energies of the HOMOs exactly match the negative signs of the experimental VDEs (see the text). The isosurface plots are presented only for alpha electrons with the isovalue of 0.0035.

As illustrated in the insets of Figs. 3(a) and (b), the undoped clusters of Ag_{18}^- and Ag_{19}^- form 3D structures. It is obvious that the HOMOs of Ag_{18}^- and Ag_{19}^- are of 2S character, which is consistent with the jellium model predicting their electron configurations of $1S^21P^61D^{10}2S^1$ and $1S^21P^61D^{10}2S^2$ for Ag_{18}^- and Ag_{19}^-, respectively. As for the bimetallic clusters, Ag_NSc^- (N = 15, 16), the Sc atom is fully encapsulated by a silver nanocage, as seen in the insets of Figs. 3(c) and (d). The optimized structure of $Ag_{15}Sc^-$ is closer to a spherical shape than that of $Ag_{16}Sc^-$. The HOMO of $Ag_{15}Sc^-$ delocalizes over the metal framework and is clearly of 2S character, suggesting that the jellium model is a proper approximation for describing the electronic configuration of this cluster. In contrast, it seems from the isosurface plot of Fig. 3(d) that the spatial character of the HOMO of $Ag_{16}Sc^-$ cannot be explained by 2S SAO only, which will be discussed below.

To discuss the characters of the HOMOs formed in these clusters more quantitatively, we further performed theoretical calculations of photoelectron anisotropy parameters, β, by employing ezDyson 5.0 developed by Gozem and Krylov[35,36] for calculating laboratory-frame PADs. In the program, a Dyson orbital, defined as the overlap between electronic wave functions with N and N−1 electrons, can be calculated based on electronic structure calculations by the equation-of-motion coupled cluster methods. While Dyson orbitals are necessary for rigorously evaluating photoelectron matrix elements, the computational costs for the present systems are very high. Therefore, we substitute Kohn-Sham orbitals for Dyson orbitals, assuming that only a single electron is involved in photodetachment process and that electronic relaxation upon photodetachment can be neglected. Here, we used the Q-Chem 5.4 package[37] to perform DFT calculations with the same functional as mentioned above to obtain Kohn-Sham orbitals based on the optimized geometries illustrated in Figs. 3(a)–(d); the basis sets used were LanL2DZ for both

Ag and Sc. The Kohn-Sham orbitals thus obtained were transferred into ezDyson 5.0 for the calculations of β values, where we assumed a plane wave for photoelectron wave function, as is normally employed for photodetachment processes for atomic and molecular anions;[38] we truncated l_{max}, the maximum number of the orbital angular momentum, at 5 (i.e., h-wave) in the expansion of the spherical harmonics. For just reference, we first computed the β value for the photodetachment from 5s atomic orbital of Ag^- and found it exactly to be 2 as expected for an ideal s orbital. The electron affinity of Ag, on the other hand, was calculated to be 1.24 eV, which is in good agreement with the experimental value of 1.302 ± 0.007 eV.[39]

The results of the β values calculated for all the clusters are summarized in Table 1 along with the experimental ones. Although the theoretical treatment for evaluating the photoelectron matrix elements is not sophisticated, the large positive values of 1.52 ± 0.03 and 1.58 ± 0.11 measured for Ag_{18}^- and $Ag_{15}Sc^-$, respectively, are reproduced by the calculation: 1.95 and 1.57 for Ag_{18}^- and $Ag_{15}Sc^-$, respectively. As for Ag_{19}^- and $Ag_{16}Sc^-$, the calculation overestimates the experimental values by ~0.7, although it qualitatively reproduces the positive anisotropy in PAD observed by the experiment. We also examined different combinations of functionals and basis sets to estimate uncertainties in the calculated β values and VDEs for all the clusters. The results are summarized in Table S1 of the Supporting Information. It was found that the calculated β values and VDEs presented in Table 1 are reproduced within ~0.05 and ~0.1 eV, respectively.

As mentioned already, only p_z-wave ($l = 1$, $m = 0$) is emitted from s orbitals ($l = 0$, $m = 0$) in single-photon detachment for atomic anions with linearly-polarized light. Here, we explore characters of photoelectrons detached from 2S SAOs of the present clusters by partial wave analysis. Figures 4(a)–(d) show the contribution of s-, p-, d-, f-, g-, and h-waves in the calculated photoelectron wave functions in the photoelectron kinetic energy (PKE) range from 0 to 2 eV;

the vertical dashed lines indicate the PKEs corresponding to the peak energies of the photoelectron spectra presented in Figs. 2(a)–(d), i.e., PKE = $h\nu$ − VDE. Figs. 4(a) and (b) show that p_z-wave (l = 1, m = 0) is dominant over the other partial waves, which accounts for the significantly large positive β values of 1.95 and 1.77 calculated for Ag_{18}^- and Ag_{19}^-, respectively. This is qualitatively consistent with PAD observed for s atomic orbitals. However, unlike the atomic case, clusters can emit partial waves other than p_z-wave (l = 1, m = 0), as they are not spherically symmetric. This behavior is seen in Figs. 4(a) and (b), where s-wave is predicted only in the photodetachment threshold, which reflects Wigner's threshold law,[40] and the contributions of the partial waves with $l \geq 2$ gradually increase as PKE goes up.

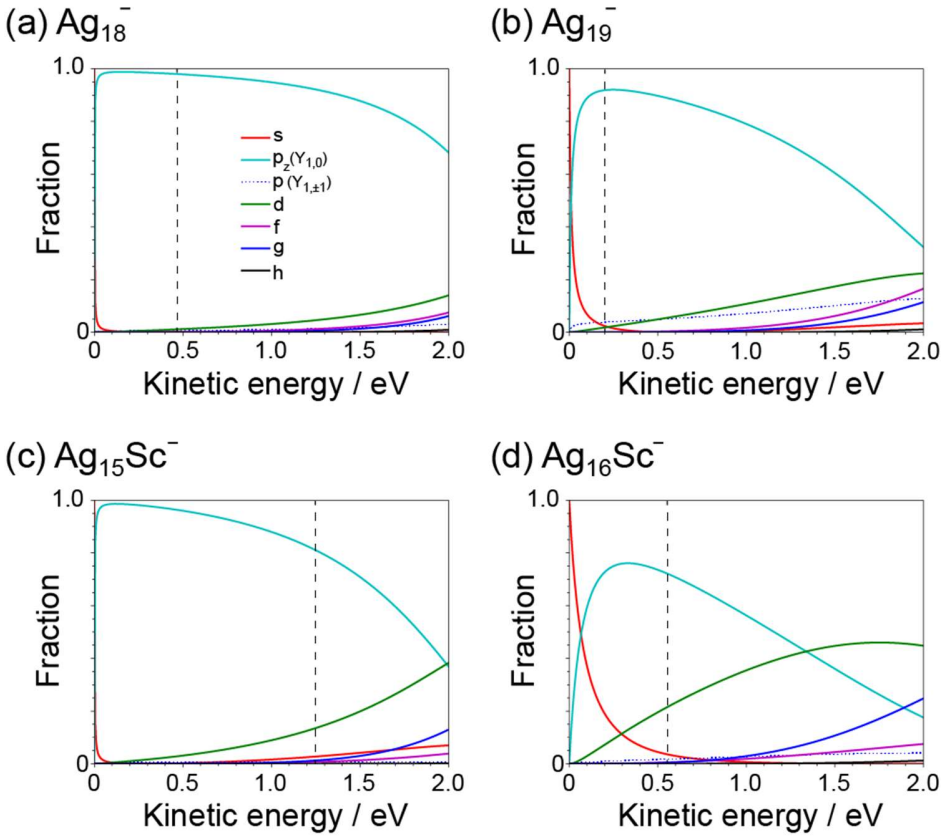

Figure 4. Photoelectron partial wave analysis for (a) Ag_{18}^-, (b) Ag_{19}^-, (c) $Ag_{15}Sc^-$, and (d) $Ag_{16}Sc^-$ from 0 to 2 eV in photoelectron kinetic energy (PKE). The vertical dashed lines indicate the PKEs that correspond to the peak energies of their photoelectron spectra presented in Figs. 2(a)–(d).

As shown in Figs. 4(c) and (d), it is clear for $Ag_{15}Sc^-$ and $Ag_{16}Sc^-$ that p_z-wave (l = 1, m = 0) is also dominant, indicating photodetachment from SAOs with S character. This is seemingly consistent with the jellium model, where the outermost SAO is predicted to be 2S for both clusters. However, examination of Figs. 4(c) and (d) reveals that the contributions of d-waves (l = 2) are noticeable, indicating photodetachment from SAOs with P and/or F character(s) according to the selection rule of $\Delta l = \pm 1$. Especially for $Ag_{16}Sc^-$, the contribution of s-wave is

256 also large in 0 – 0.5 eV, which implies that the HOMO is of P character to a certain extent. In
257 addition, Fig. 4(d) shows that the contributions of g-waves (l = 4) are not negligible in the higher
258 PKE region, suggesting that the HOMO of $Ag_{16}Sc^-$ has a F character. In fact, such a F character
259 (i.e., $1F_{z^3}$) is evident in the orbital shape shown in Fig. 3(d). Thus, the partial wave analysis
260 reveals the contribution of P and F SAOs for the outermost SAO of $Ag_{16}Sc^-$, which may cause
261 large reduction of the corresponding β value (see Table 1).

262 Finally, we address a heteroatom-doping effect on discrete energy levels of SAOs. As
263 seen in the photoelectron spectra observed for Ag_{18}^- (Fig. 2(a)) and $Ag_{15}Sc^-$ (Fig. 2(c)), the
264 former VDE, 2.60 eV, is significantly higher than that for the latter, 1.82 eV, indicating that the
265 quantized energy level of the singly occupied 2S orbital is destabilized upon Sc doping; it is also
266 visualized from Figs. 1(d) and (h), where the ring diameter for $Ag_{15}Sc^-$ is much larger than that
267 for Ag_{18}^-. Lievens and co-workers[41] discussed such a doping effect on SAOs using a two-step
268 spherical jellium model, where the authors assumed that when a foreign atom is embedded in the
269 center of a host metal 3D cage, the energy levels of SAOs are subject to change depending on
270 their orbital angular momenta (S, P, D, …) due to the difference in electronegativity (EN)
271 between the dopant and the host metal. The situation is schematically illustrated in Fig. 5.

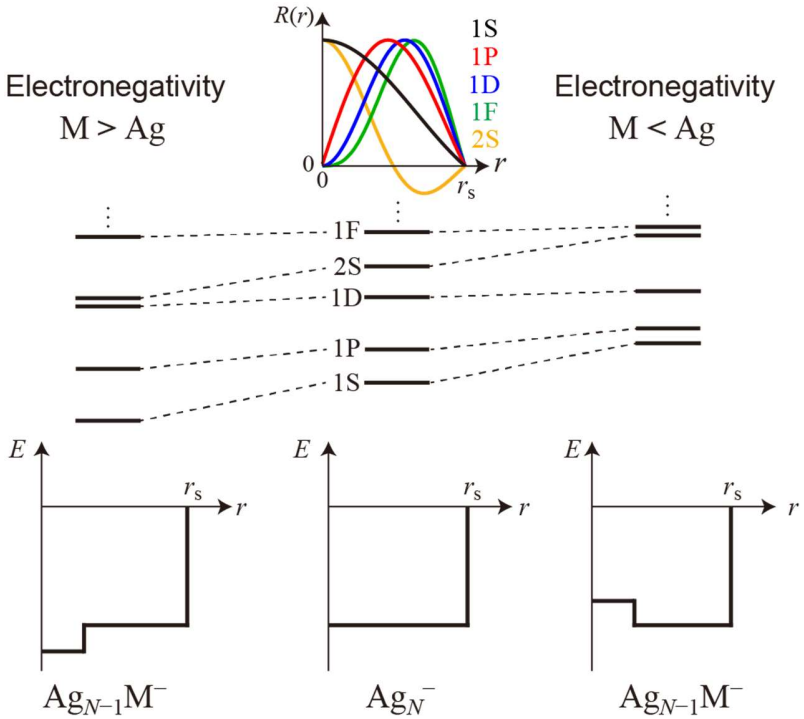

272

273 **Figure 5**. Schematic diagram of the energy levels of SAOs in undoped silver cluster anions,
274 Ag_N^-, and hetero-atom-doped silver cluster anions, $Ag_{N-1}M^-$, where we assume the clusters'
275 geometries to be a sphere with a radius of r_s. Radial parts, $R(r)$, of 1S, 1P, 1D, 1F, and 2S SAOs,
276 $R(r)$, are also shown schematically in the upper middle. For simplicity, $R(r)$ is set as 0 at $r = r_s$.

277

278 When the central foreign atom is more/less electronegative than the host metal, the
279 potential well becomes more/less attractive at the center of the doped cluster, leading to
280 stabilization/destabilization of SAOs that have larger/smaller amplitudes at the center.
281 Schematical representations of radial parts of 1S, 1P, 1D, 2S, 1F SAOs are shown in the upper
282 middle of Fig. 5, where the amplitudes of 1S and 2S are the highest at the center, whereas the
283 maximum amplitudes of 1P, 1D, and 1F appear away from the center. Consequently, 1S and 2S
284 are more stabilized/destabilized upon doping with a central heteroatom with higher/lower EN.
285 Since the ENs of Sc and Ag, defined by Allen and coworkers, [19] are 1.19 and 1.87, respectively,

the 2S orbital energy is subject to increase, as shown in the right panel of Fig. 5. The observation of lower VDEs for Ag_NSc^- (N = 15, 16) relative to those obtained for Ag_N^- (N = 18, 19) is therefore consistent with this picture. The destabilization of the 2S level results in orbital mixing between 2S and 1F SAOs, which has been found for $Ag_{16}Sc^-$ as discussed above. The two outermost valence electrons favor occupying such a mixed SAO, making its geometry of $Ag_{16}Sc^-$ deformed from a nearly spherical shape, as manifested in the optimized structure shown Fig. 3(d).

In conclusion, we have clearly visualized photoelectron distributions detached from Sc-doped and undoped silver cluster anions with 19 and 20 valence electrons, Ag_NSc^- (N = 15 and 16) and Ag_N^- (N = 18 and 19). Referring to the experimental VDEs, their optimized structures have been determined by DFT calculations, where we have found that a Sc atom is fully encapsulated in the silver framework for the doped clusters. PAD observed for $Ag_{15}Sc^-$ exhibited significantly high anisotropy with more electrons emitted parallel to the laser polarization, which was also found for a valence isoelectronic counterpart of Ag_{18}^-. The calculation of laboratory-frame PAD using ezDyson qualitatively supports the experimental results of the 19-e clusters. The partial wave analysis of the photoelectron wave function has revealed that p_z-wave (l = 1, m = 0) is a dominant partial wave for both cases, indicating that the electron to be detached is of S character. This is consistent with the electronic configuration of $1S^21P^61D^{10}2S^1$ predicted by the spherical jellium model, although weak P and/or F characters are suggested in the HOMO of $Ag_{15}Sc^-$. On the other hand, the positive anisotropy decreases for $Ag_{16}Sc^-$ compared with the other cluster anions. The partial wave decomposition has suggested that the reduction in the β parameter is caused by the orbital mixing between 2S and P and/or F SAOs. Orbital energy shift upon heteroatom doping in SAOs, proposed by the two-step jellium model, has also been

identified. The present work provides the first, to the best of our knowledge, experimental and theoretical verifications of the formation of SAOs in bimetallic clusters via photoelectron angular anisotropy. The application of the present methodology to other systems is straightforward and such investigations are in progress in our group.

EXPERIMENTAL METHODS

The apparatus is almost identical to the one reported previously.[21] Briefly, a magnetron-sputtering cluster ion source followed by a quadrupole mass filter[17] produces a continuous beam of size-selected metal cluster anions, which is transformed into ion bunches with a potential switch driven by a high voltage (+600 V) pulser operating at a repetition rate of ~150 kHz with a duty cycle of ~50%. The quasi-continuous anion beam is introduced to a photoelectron imaging spectrometer with the velocity mapping imaging (VMI) configuration,[42] where the anions are irradiated with a continuous-wave (CW) beam of a linearly-polarized, 404-nm (3.07-eV) laser diode with an average output of approximately 400 mW. Photoelectrons are accelerated by the VMI electrodes toward a dual microchannel plate (the effective diameter is 44 mmϕ) backed with a phosphor screen (P43). A two-dimensional (2D) projection of the three-dimensional (3D) distribution of the photoelectrons on the phosphor screen is captured with a complementary metal oxide semiconductor camera (1920×1080 pixels). The camera acquires the 2D projection for 500 ms, where the image acquisitions were repeated to achieve an acceptable signal to noise ratio. The incident anion beam itself creates low-energy electrons as it impinges on the inner walls of the VMI electrodes. To remove such background noises, a laser-off image is subtracted from a laser-on image. The image after the subtraction is further processed to reconstruct the original 3D distribution by a polar-onion-peeling (POP) algorithm.[43] Photoelectron kinetic

energy is calibrated with VDE of Ag_3^- (2.43 eV).[39] The energy resolution ($\Delta E/E$) is 4% (0.07 eV) at E = 1.77 eV.

AUTHOR INFORMATION

Corresponding Authors:

Takuya Horio − Department of Chemistry, Faculty of Science, Kyushu University, 744 Motooka, Nishi-ku, Fukuoka 819-0395, Japan; orcid.org/0000-0002-5769-6155;

Email: horio@chem.kyushu-univ.jp

Akira Terasaki − Department of Chemistry, Faculty of Science, Kyushu University, 744 Motooka, Nishi-ku, Fukuoka 819-0395, Japan; orcid.org/0000-0001-8293-0698;

Email: terasaki@chem.kyushu-univ.jp

Authors:

Kento Minamikawa† − Department of Chemistry, Faculty of Science, Kyushu University, 744 Motooka, Nishi-ku, Fukuoka 819-0395, Japan; Present address: Toshiba Corporate Research & Development Center, Komukai Toshiba-cho, Saiwai-ku, Kawasaki-shi, 212-8582, Japan

Tasuku Nishizato† − Department of Chemistry, Faculty of Science, Kyushu University, 744 Motooka, Nishi-ku, Fukuoka 819-0395, Japan

Haruki Hashimoto − Department of Chemistry, Faculty of Science, Kyushu University, 744 Motooka, Nishi-ku, Fukuoka 819-0395, Japan

Kazuaki Matsumoto − Department of Chemistry, Faculty of Science, Kyushu University, 744 Motooka, Nishi-ku, Fukuoka 819-0395, Japan.

Masashi Arakawa − Department of Chemistry, Faculty of Science, Kyushu University, 744 Motooka, Nishi-ku, Fukuoka 819-0395, Japan; orcid.org/0000-0002-5954-8893

†These authors contributed equally.

Notes

The authors declare no competing financial interests.

ASSOCIATED CONTENT

Supporting Information: Photoelectron anisotropy parameters, β, and the vertical detachment energies (VDEs) calculated for Ag_{18}^-, Ag_{19}^-, $Ag_{15}Sc^-$, and $Ag_{16}Sc^-$ using different combinations of functionals and basis sets.

ACKNOWLEDGMENTS

This work was supported by Grants-in-Aid for Scientific Research (A) (JP18H03901 and JP22H00317), Scientific Research (B) (JP22H02036), and Challenging Research (Exploratory) (JP20K21177 and JP22K19009) from the Japan Society for Promotion of Science (JSPS), the Asahi Glass Foundation, Iketani Science and Technology Foundation, and the Research Project of Genesis Research Institute, Inc. The authors are grateful to Rin Nomi and Yuta Suzuki for

their experimental and computational assistance. The computational work was carried out by the computer facilities at Research Institute for Information Technology, Kyushu University.

REFERENCES

(1) Knight, W. D.; Clemenger, K.; de Heer, W. A.; Saunders, W. A.; Chou, M. Y.; Cohen, M. L. Electronic Shell Structure and Abundances of Sodium Clusters. *Phys. Rev. Lett.* **1984**, *52* (24), 2141–2143.

(2) de Heer, W. A. The Physics of Simple Metal Clusters: Experimental Aspects and Simple Models. *Rev. Mod. Phys.* **1993**, *65* (3), 611–676.

(3) Leopold, D. G.; Ho, J.; Lineberger, W. C. Photoelectron Spectroscopy of Mass-selected Metal Cluster Anions. I. Cu_n^-, n =1–10. *J. Chem. Phys.* **1987**, *86* (4), 1715–1726.

(4) McHugh, K. M.; Eaton, J. G.; Lee, G. H.; Sarkas, H. W.; Kidder, L. H.; Snodgrass, J. T.; Manaa, M. R.; Bowen, K. H. Photoelectron Spectra of the Alkali Metal Cluster Anions: $Na_{n=2-5}^-$, $K_{n=2-7}^-$, $Rb_{n=2-3}^-$, and $Cs_{n=2-3}^-$. *J. Chem. Phys.* **1989**, *91* (6), 3792–3793.

(5) Taylor, K. J.; Pettiette-Hall, C. L.; Cheshnovsky, O.; Smalley, R. E. Ultraviolet Photoelectron Spectra of Coinage Metal Clusters. *J. Chem. Phys.* **1992**, *96* (4), 3319–3329.

(6) Handschuh, H.; Cha, C.; Bechthold, P. S.; Ganteför, G.; Eberhardt, W. Electronic Shells or Molecular Orbitals: Photoelectron Spectra of Ag_n^- Clusters. *J. Chem. Phys.* **1995**, *102* (16), 6406–6422.

(7) Wrigge, G.; Hoffmann, M. A.; von Issendorff, B. Photoelectron Spectroscopy of Sodium Clusters: Direct Observation of the Electronic Shell Structure. *Phys. Rev. A* **2002**, *65* (6), 063201.

(8) Häkkinen, H.; Yoon, B.; Landman, U.; Li, X.; Zhai, H.-J.; Wang, L.-S. On the Electronic and Atomic Structures of Small Au_N^- (N = 4−14) Clusters: A Photoelectron Spectroscopy and Density-Functional Study. *J. Phys. Chem. A* **2003**, *107* (32), 6168–6175.

(9) Castleman, A. W.; Khanna, S. N. Clusters, Superatoms, and Building Blocks of New Materials. *J. Phys. Chem. C* **2009**, *113* (7), 2664–2675.

(10) Aikens, C. M.; Jin, R.; Roy, X.; Tsukuda, T. From Atom-Precise Nanoclusters to Superatom Materials. *J. Chem. Phys.* **2022**, *156* (17), 170401.

(11) Kappes, M. M.; Radi, P.; Schär, M.; Schumacher, E. Probes for Electronic and Geometrical Shell Structure Effects in Alkali-Metal Clusters. Photoionization Measurements on K_xLi, K_xMg and K_xZn ($x < 25$). *Chem. Phys. Lett.* **1985**, *119* (1), 11–16.

(12) Nakajima, A.; Hoshino, K.; Naganuma, T.; Sone, Y.; Kaya, K. Ionization Potentials of Aluminum–Sodium Bimetallic Clusters ($Al_n Na_m$). *J. Chem. Phys.* **1991**, *95* (10), 7061–7066.

(13) Pyykkö, P.; Runeberg, N. Icosahedral WAu_{12}: A Predicted Closed-Shell Species, Stabilized by Aurophilic Attraction and Relativity and in Accord with the 18-Electron Rule. *Angew. Chem. Int. Ed.* **2002**, *41* (12), 2174.

(14) Li, X.; Kiran, B.; Li, J.; Zhai, H.-J.; Wang, L.-S. Experimental Observation and Confirmation of Icosahedral $W@Au_{12}$ and $Mo@Au_{12}$ Molecules. *Angew. Chem. Int. Ed.* **2002**, *41* (24), 4786–4789.

(15) Neukermans, S.; Janssens, E.; Tanaka, H.; Silverans, R. E.; Lievens, P. Element- and Size-Dependent Electron Delocalization in $Au_N X^+$ Clusters (X = Sc, Ti, V, Cr, Mn, Fe, Co, Ni). *Phys. Rev. Lett.* **2003**, *90* (3), 033401.

(16) Janssens, E.; Neukermans, S.; Nguyen, H. M. T.; Nguyen, M. T.; Lievens, P. Quenching of the Magnetic Moment of a Transition Metal Dopant in Silver Clusters. *Phys. Rev. Lett.* **2005**, *94* (11), 113401.

(17) Sarugaku, S.; Arakawa, M.; Kawano, T.; Terasaki, A. Electronic and Geometric Effects on Chemical Reactivity of 3d-Transition-Metal-Doped Silver Cluster Cations toward Oxygen Molecules. *J. Phys. Chem. C* **2019**, *123* (42), 25890–25897.

(18) Minamikawa, K.; Sarugaku, S.; Arakawa, M.; Terasaki, A. Electron Counting in Cationic and Anionic Silver Clusters Doped with a 3d Transition-Metal Atom: Endo- *vs.* Exohedral Geometry. *Phys. Chem. Chem. Phys.* **2022**, *24* (3), 1447–1455.

(19) Mann, J. B.; Meek, T. L.; Knight, E. T.; Capitani, J. F.; Allen, L. C. Configuration Energies of the d-Block Elements. *J. Am. Chem. Soc.* **2000**, *122* (21), 5132–5137.

(20) Gilmour, J. T. A.; Gaston, N. Design of Superatomic Systems: Exploiting Favourable Conditions for the Delocalisation of d-Electron Density in Transition Metal Doped Clusters. *Phys. Chem. Chem. Phys.* **2020**, *22* (33), 18585–18594.

(21) Horio, T.; Minamikawa, K.; Nishizato, T.; Hashimoto, H.; Matsumoto, K.; Arakawa, M.; Terasaki, A. Photoelectron Imaging of Size-Selected Metal Cluster Anions in a Quasi-Continuous Mode. *Rev. Sci. Instrum.* **2022**, *93* (8), 083302.

(22) Cooper, J.; Zare, R. N. Angular Distribution of Photoelectrons. *J. Chem. Phys.* **1968**, *48* (2), 942–943.

(23) Sobhy, M. A.; Castleman, A. W. Photoelectron Imaging of Copper and Silver Mono- and Diamine Anions. *J. Chem. Phys.* **2007**, *126* (15), 154314.

(24) Bartels, C.; Hock, C.; Huwer, J.; Kuhnen, R.; Schwöbel, J.; von Issendorff, B. Probing the Angular Momentum Character of the Valence Orbitals of Free Sodium Nanoclusters. *Science* **2009**, *323* (5919), 1323–1327.

(25) Frisch, M. J.; Trucks, G. W.; Schlegel, H. B.; Scuseria, G. E.; Robb, M. A.; Cheeseman, J. R.; Scalmani, G.; Barone, V.; Petersson, G. A.; Nakatsuji, H.; Li, X.; Caricato, M.; Marenich, A. V.; Bloino, J.; Janesko, B. G.; Gomperts, R.; Mennucci, B.; Hratchian, H. P.; Ortiz, J. V.; Izmaylov, A. F.; Sonnenberg, J. L.; Williams-Young, D.; Ding, F.; Lipparini, F.; Egidi, F.; Goings, J.; Peng, B.; Petrone, A.; Henderson, T.; Ranasinghe, D.; Zakrzewski, V. G.; Gao, J.; Rega, N.; Zheng, G.; Liang, W.; Hada, M.; Ehara, M.; Toyota, K.; Fukuda, R.; Hasegawa, J.; Ishida, M.; Nakajima, T.; Honda, Y.; Kitao, O.; Nakai, H.; Vreven, T.; Throssell, K.; Montgomery, J. A. Jr.; Peralta. J. E.; Ogliaro, F.; Bearpark, M. J.; Heyd, J. J.; Brothers, E. N.; Kudin, K. N.; Staroverov, V. N.; Keith, T. A.; Kobayashi, R.; Normand, J.; Raghavachari, K.; Rendell, A. P.; Burant, J. C.; Iyengar, S. S.; Tomasi, J.; Cossi, M.; Millam, J. M.; Klene, M.; Adamo, C.; Cammi, R.; Ochterski, J. W.; Martin, R. L.; Morokuma, K.; Farkas, O.; Foresman, J. B.; Fox, D. J.; Gaussian, Inc. , W. C. 2016. Gaussian 16, Revision C.01.

(26) Perdew, J. P. Density-Functional Approximation for the Correlation Energy of the Inhomogeneous Electron Gas. *Phys. Rev. B* **1986**, *33* (12), 8822–8824.

(27) Becke, A. D. Density-Functional Exchange-Energy Approximation with Correct Asymptotic Behavior. *Phys. Rev. A* **1988**, *38* (6), 3098–3100.

(28) Wachters, A. J. H. Gaussian Basis Set for Molecular Wavefunctions Containing Third-Row Atoms. *J. Chem. Phys.* **1970**, *52* (3), 1033–1036.

(29) Hay, P. J. Gaussian Basis Sets for Molecular Calculations. The Representation of 3 *d* Orbitals in Transition-metal Atoms. *J. Chem. Phys.* **1977**, *66* (10), 4377–4384.

(30) Raghavachari, K.; Trucks, G. W. Highly Correlated Systems. Excitation Energies of First Row Transition Metals Sc–Cu. *J. Chem. Phys.* **1989**, *91* (2), 1062–1065.

(31) Hay, P. J.; Wadt, W. R. *Ab Initio* Effective Core Potentials for Molecular Calculations. Potentials for the Transition Metal Atoms Sc to Hg. *J. Chem. Phys.* **1985**, *82* (1), 270–283.

(32) Yin, B.; Du, Q.; Geng, L.; Zhang, H.; Luo, Z.; Zhou, S.; Zhao, J. Superatomic Signature and Reactivity of Silver Clusters with Oxygen: Double Magic Ag_{17}^- with Geometric and Electronic Shell Closure. *CCS Chemistry* **2021**, *3* (12), 219–229.

(33) Tozer, D. J.; Handy, N. C. Improving Virtual Kohn–Sham Orbitals and Eigenvalues: Application to Excitation Energies and Static Polarizabilities. *J. Chem. Phys.* **1998**, *109* (23), 10180–10189.

(34) Akola, J.; Manninen, M.; Häkkinen, H.; Landman, U.; Li, X.; Wang, L.-S. Photoelectron Spectra of Aluminum Cluster Anions: Temperature Effects and *Ab Initio* Simulations. *Phys. Rev. B* **1999**, *60* (16), R11297–R11300.

(35) Gozem, S.; Gunina, A. O.; Ichino, T.; Osborn, D. L.; Stanton, J. F.; Krylov, A. I. Photoelectron Wave Function in Photoionization: Plane Wave or Coulomb Wave? *J. Phys. Chem. Lett.* **2015**, *6* (22), 4532–4540.

(36) Gozem, S.; Krylov, A. I. The *EzSpectra* Suite: An Easy-to-use Toolkit for Spectroscopy Modeling. *WIREs Computational Molecular Science* **2022**, *12* (2).

(37) Epifanovsky, E.; Gilbert, A. T. B.; Feng, X.; Lee, J.; Mao, Y.; Mardirossian, N.; Pokhilko, P.; White, A. F.; Coons, M. P.; Dempwolff, A. L.; Gan, Z.; Hait, D.; Horn, P. R.; Jacobson, L. D.; Kaliman, I.; Kussmann, J.; Lange, A. W.; Lao, K. U.; Levine, D. S.; Liu, J.; McKenzie, S. C.; Morrison, A. F.; Nanda, K. D.; Plasser, F.; Rehn, D. R.; Vidal, M. L.; You, Z.-Q.; Zhu, Y.; Alam, B.; Albrecht, B. J.; Aldossary, A.; Alguire, E.; Andersen, J. H.; Athavale, V.; Barton, D.; Begam, K.; Behn, A.; Bellonzi, N.; Bernard, Y. A.; Berquist, E. J.; Burton, H. G. A.; Carreras, A.; Carter-Fenk, K.; Chakraborty, R.; Chien, A. D.; Closser, K. D.; Cofer-Shabica, V.; Dasgupta, S.; de Wergifosse, M.; Deng, J.; Diedenhofen, M.; Do, H.; Ehlert, S.; Fang, P.-T.; Fatehi, S.; Feng, Q.; Friedhoff, T.; Gayvert, J.; Ge, Q.; Gidofalvi, G.; Goldey, M.; Gomes, J.; González-Espinoza, C. E.; Gulania, S.; Gunina, A. O.; Hanson-Heine, M. W. D.; Harbach, P. H. P.; Hauser, A.; Herbst, M. F.; Hernández Vera, M.; Hodecker, M.; Holden, Z. C.; Houck, S.; Huang, X.; Hui, K.; Huynh, B. C.; Ivanov, M.; Jász, Á.; Ji, H.; Jiang, H.; Kaduk, B.; Kähler, S.; Khistyaev, K.; Kim, J.; Kis, G.; Klunzinger, P.; Koczor-Benda, Z.; Koh, J. H.; Kosenkov, D.; Koulias, L.; Kowalczyk, T.; Krauter, C. M.; Kue, K.; Kunitsa, A.; Kus, T.; Ladjánszki, I.; Landau, A.; Lawler, K. v.; Lefrancois, D.; Lehtola, S.; Li, R. R.; Li, Y.-P.; Liang, J.; Liebenthal, M.; Lin, H.-H.; Lin, Y.-S.; Liu, F.; Liu, K.-Y.; Loipersberger, M.; Luenser, A.; Manjanath, A.; Manohar, P.; Mansoor, E.; Manzer, S. F.; Mao, S.-P.; Marenich, A. v.; Markovich, T.; Mason, S.; Maurer, S. A.; McLaughlin, P. F.; Menger, M. F. S. J.; Mewes, J.-M.; Mewes, S. A.; Morgante, P.; Mullinax, J. W.; Oosterbaan, K. J.; Paran, G.; Paul, A. C.; Paul, S. K.; Pavošević, F.; Pei, Z.; Prager, S.; Proynov, E. I.; Rák, Á.; Ramos-Cordoba, E.; Rana, B.; Rask, A. E.; Rettig, A.; Richard, R. M.; Rob, F.; Rossomme, E.; Scheele, T.; Scheurer, M.; Schneider, M.; Sergueev, N.; Sharada, S. M.; Skomorowski, W.; Small, D. W.; Stein, C. J.; Su, Y.-C.; Sundstrom, E. J.; Tao, Z.; Thirman, J.; Tornai, G. J.; Tsuchimochi, T.; Tubman, N. M.; Veccham, S. P.; Vydrov, O.; Wenzel, J.; Witte, J.; Yamada, A.; Yao, K.; Yeganeh, S.; Yost, S. R.; Zech, A.; Zhang, I. Y.; Zhang, X.; Zhang, Y.; Zuev, D.; Aspuru-Guzik, A.; Bell, A. T.; Besley, N. A.; Bravaya, K. B.; Brooks, B. R.; Casanova, D.; Chai, J.-D.; Coriani, S.; Cramer, C. J.; Cserey, G.; DePrince, A. E.; DiStasio, R. A.; Dreuw, A.; Dunietz, B. D.; Furlani, T. R.; Goddard, W. A.; Hammes-Schiffer, S.; Head-Gordon, T.; Hehre, W. J.; Hsu, C.-P.; Jagau, T.-C.; Jung, Y.; Klamt, A.; Kong, J.; Lambrecht, D. S.; Liang, W.; Mayhall, N. J.; McCurdy, C. W.; Neaton, J. B.; Ochsenfeld, C.; Parkhill, J. A.; Peverati, R.; Rassolov, V. A.; Shao, Y.; Slipchenko, L. v.; Stauch, T.; Steele, R. P.; Subotnik, J. E.; Thom, A. J. W.; Tkatchenko, A.; Truhlar, D. G.; van Voorhis, T.; Wesolowski, T. A.; Whaley, K. B.; Woodcock, H. L.; Zimmerman, P. M.; Faraji, S.; Gill, P. M. W.; Head-Gordon, M.; Herbert, J. M.; Krylov, A. I. Software for the Frontiers of Quantum Chemistry: An Overview of Developments in the Q-Chem 5 Package. *J. Chem. Phys.* **2021**, *155* (8), 084801.

(38) Sanov, A. Laboratory-Frame Photoelectron Angular Distributions in Anion Photodetachment: Insight into Electronic Structure and Intermolecular Interactions. *Annu. Rev. Phys. Chem.* **2014**, *65* (1), 341–363.

(39) Ho, J.; Ervin, K. M.; Lineberger, W. C. Photoelectron Spectroscopy of Metal Cluster Anions: Cu_n^-, Ag_n^-, and Au_n^-. *J. Chem. Phys.* **1990**, *93* (10), 6987–7002.

(40) Wigner, E. P. On the Behavior of Cross Sections Near Thresholds. *Phys. Rev.* **1948**, *73* (9), 1002–1009.

(41) Janssens, E.; Neukermans, S.; Lievens, P. Shells of Electrons in Metal Doped Simple Metal Clusters. *Curr. Opin. Solid State Mater. Sci.* **2004**, *8* (3–4), 185–193.

(42) Eppink, A. T. J. B.; Parker, D. H. Velocity Map Imaging of Ions and Electrons Using Electrostatic Lenses: Application in Photoelectron and Photofragment Ion Imaging of Molecular Oxygen. *Rev. Sci. Instrum.* **1997**, *68* (9), 3477–3484.

(43) Roberts, G. M.; Nixon, J. L.; Lecointre, J.; Wrede, E.; Verlet, J. R. R. Toward Real-Time Charged-Particle Image Reconstruction Using Polar Onion-Peeling. *Rev. Sci. Instrum.* **2009**, *80* (5), 053104.